First-principles calculations of the vibrational and thermal properties of the type-I clathrates $Ba_8Ga_{16}Si_xGe_{30-x}$ and $Sr_8Ga_{16}Si_xGe_{30-x}$

Emmanuel N. Nenghabi and Charles W. Myles
Department of Physics, Texas Tech University, MS 1051, Lubbock, Texas 79409, USA
(Received 28 June 2008; published 5 November 2008)

We have performed density-functional calculations of the vibrational and thermal properties of some of the type-I semiconductor clathrate "alloys" $Ba_8Ga_{16}Si_xGe_{30-x}$ and $Sr_8Ga_{16}Si_xGe_{30-x}$ as a function of Si composition x. We find that the guest-atoms Ba and Sr produce localized vibrational modes lying below 80 cm^{-1}, which tend to reduce the acoustic bandwidth of the host material. Our results also predict an upshift in the flat optic modes of the host framework as the Si content of the lattice increases and that the guest-atom-associated Einstein temperature in these materials varies with x. Our calculated isotropic atomic displacement parameters as functions of temperature for the guest Ba and Sr atoms in these clathrates predict that Sr has a larger isotropic displacement parameter than Ba, thus suggesting that Sr should be more efficient than Ba in suppressing the thermal conductivity. We have also calculated the temperature dependences of the vibrational contributions to the specific heat, the entropy, and the Helmholtz free energy in these materials. We find that the heat capacities of these clathrates increase smoothly with temperature and approach the Dulong-Petit value at around room temperature. As expected, we also find that in these materials, there is also a slight x dependence of the heat capacity, free energy, and vibrational entropy.

DOI: 10.1103/PhysRevB.78.195202 PACS number(s): 71.20.Nr, 72.80.Cw, 71.15.Mb

I. INTRODUCTION

Because of their very interesting properties, germanium clathrate compounds have attracted considerable theoretical and experimental interest over the past several years. These materials are also interesting technologically, mostly because of their potential applications in thermoelectric devices.[1–5] The thermoelectric performance of a material is given by the dimensionless figure of merit, usually denoted as ZT. Here, T is the absolute temperature and $Z=S^2\sigma/\kappa$, where S is the Seebeck coefficient, σ is the electrical conductivity, and κ is the thermal conductivity. The larger the value of ZT, the more efficient is the thermoelectric device.[6,7] At present, the best materials for thermoelectric applications are semiconductors which have low thermal conductivities. For example, some promising materials are binary alloys with complex unit cells and relatively heavy atoms, such as antimony telluride or bismuth telluride.

An ideal thermoelectric material should have the electronic properties of a crystalline solid and the thermal properties of a glass. This concept was first proposed by Slack[8,9] and is known as the "phonon glass electron crystal" (PGEC) model. Most materials with excellent potential for thermoelectric applications, including clathrate semiconductors, have cages in which impurity or "guest" atoms are encapsulated. These guests vibrate ("rattle") at very low frequencies inside the host cages, thereby scattering the heat-carrying acoustic phonons of the host and lowering the thermal conductivity. The guest atoms or "rattlers" usually have little effect on the conduction electrons of the host, potentially making such materials good PGEC's.[10–12]

The motivation for much of the recent research on clathrate materials has been the search for a clathrate with good thermoelectric characteristics.[1] In addition to the fact that the guest atoms can change the physical and chemical properties of the host framework, in the clathrates, other atoms can be alloyed on the framework sites and this can also cause a rich variety of changes in the material properties. In this paper, we report the results of calculations of the lattice vibrational spectra and the thermal properties of some of the type-I semiconductor clathrate alloys $Ba_8Ga_{16}Si_xGe_{30-x}$ and $Sr_8Ga_{16}Si_xGe_{30-x}$ as a function of Si composition x.

These are very complex materials. Reference 1 discusses the details of how they are synthesized in the laboratory and the effects of the different atomic species on the material thermoelectric properties. We find that Ba and Sr guests in these materials have low-lying vibrational modes, so that their contributions to the heat capacity, the entropy, and the free energy are negligible. However, we of course expect that the guest-atom contributions to the thermal properties of these materials will be affected by the substitutional silicon atoms on the host framework lattice. The presence of the Si, Ga, and Ge atoms on the lattice framework in these materials makes it impossible to construct a structural model with high symmetry. This in turn makes vibrational or phonon calculations difficult.

In order to simplify this problem, following our previous calculations of the structural and electronic properties of $Ba_8Ga_{16}Si_xGe_{30-x}$ and $Sr_8Ga_{16}Si_xGe_{30-x}$,[13] to obtain the results discussed in the present paper, we have used the *same* model unit cell as we used in Ref. 13. In this model, the *initial configuration* of atoms (the *starting point* for our calculations before the structural optimization of the lattice, which is summarized below) is one in which two Ba or Sr guest atoms are placed on the 2*a* sites (in the smaller cages) and the remaining six Ba or Sr guests are placed on the 6*d* sites (in the larger cages). Further, in this model, the Ga atoms are initially placed on the following Wyckoff sites:[1] three on 6*c* sites, one on a 16*i* site, and 12 on 24*k* sites. Also, in this model, three Si atoms are initially placed on 6*c* sites and the others are initially placed on 16*i* sites. The Ge atoms in this model are initially placed on the remaining empty

Wyckoff sites of the unit cell. These models are not centrosymmetric. However, many other symmetry properties are preserved.

Understanding the vibrational (phonon) dispersion spectrum of a material is very important for obtaining an understanding of its transport and thermal properties. Using first-principles density-functional-based techniques within the harmonic approximation, we have calculated the vibrational modes of $Ba_8Ga_{16}Si_xGe_{30-x}$ and $Sr_8Ga_{16}Si_xGe_{30-x}$ for some values of x. Using eigenvector analyses, we have also been able to identify the vibrational modes of the Ba and Sr guests and to study how these modes affect the acoustic bandwidth of the host. We have also calculated the temperature-dependent isotropic mean-square displacement amplitudes (U_{iso}) and Einstein temperatures (θ_E or $\theta_{E\text{-ave}}$) of Ba and Sr in these materials. Finally, for these materials, we have calculated the temperature dependences of the specific-heat capacities at constant volume, the entropy, and the Helmholtz free energy.

II. THEORETICAL APPROACH

In this paper, we present the results of first-principles density-functional-based calculations of the vibrational and thermal properties of $Ba_8Ga_{16}Si_xGe_{30-x}$ and $Sr_8Ga_{16}Si_xGe_{30-x}$. In what follows, these clathrate alloys will sometimes be denoted as $A_8Ga_{16}Si_xGe_{30-x}$ (with A=Ba or Sr). We present results for materials with Si compositions x =0, 5, and 15, although other x values are certainly possible. The space-group symmetry of these materials is $Pm3n$. Following our previous work,[13] we retain cubic symmetry in all of our calculations since nonsymmetric crystallography is very difficult to model theoretically.[14] We have used the generalized gradient approximation (GGA) in all of our calculations with plane waves as the basis set. Vanderbilt ultrasoft pseudopotentials[15,16] have been used, which help reduce the computational time and improve the overall accuracy for a given energy (the plane-wave cutoff was set to 150 eV). The Vienna *ab initio* simulation package (VASP) has been used with the Perdew and Wang[17] functional to approximate the exchange-correlation energy.

The first step in our calculations is the optimization of the geometry of the lattice structures and the determination of the equations of state (EOS) within the GGA. To do this, we have chosen a fixed unit-cell volume and have optimized the atomic positions with a conjugate gradient algorithm using atomic forces. This process has been repeated for several different lattice constants until the global minimum energy was obtained for each material. Because the clathrate unit cell is very large (lattice constant ~11 Å), a single unit cell has been employed in all calculations. Brillouin-zone integrations have been performed using a $4\times4\times4$ Monkhorst-Pack[18] $\boldsymbol{k}$-space grid. The resulting GGA energy versus volume function has then been fitted to the Birch-Murnaghan equation of state[19,20] to obtain the equilibrium binding energies per unit cell, unit-cell volume, bulk modulus, and the pressure derivative of bulk modulus.

The results of these structural optimization calculations[13] show that at equilibrium, the Ba or the Sr guest-atom positions in the small and large cages in $A_8Ga_{16}Si_xGe_{30-x}$ *are not* at the cage centers. This is in qualitative agreement with results obtained by others[7,21,22] for $A_8Ga_{16}Ge_{30}$ (A=Ba and Sr). We find that the guest-equilibrium positions are displaced from the cage centers by distances which range from a few hundredths to as much as a few tenths of an angstrom, depending on the guest type, cage size, and on the Si composition x. In $Ba_8Ga_{16}Si_xGe_{30-x}$, we find equilibrium Ba positions displaced from the cage centers by distances in the range 0.039–0.05 Å in the small cages and in the range 0.045–0.11 Å in the large cages. Similarly, in $Sr_8Ga_{16}Si_xGe_{30-x}$, our equilibrium Sr displacements from the cage centers are in the range 0.072–0.090 Å in the small cages and in the range 0.06–0.81 Å in the large cages. These off-center equilibrium guest positions are a type of structural or static disorder. The physical origin of this guest-atom disorder is the fact that when the guests are displaced away from the cage centers, they are closer to some of the framework atoms. In those positions, they can thus more easily form strong directional bonds to the host atoms, making it energetically favorable for the guests to remain away from the cage center.

To obtain the lattice vibrational dispersion relations starting with the GGA-optimized structure just discussed, we have calculated the dynamical matrix $D(\mathbf{q})$, where $\mathbf{q}$ is a phonon wave vector in the first Brillouin zone. The eigenvalues (squares of the vibrational frequencies) and eigenvectors were obtained by diagonalizing $D(\mathbf{q})$. This procedure has been carried out in two steps. Starting with a free-optimized unit cell with N atoms using VASP, we have determined the $3N\times3N$ $\mathbf{q}$=(000)-point force-constant matrix for the primitive cell in the harmonic approximation. To do this, each atom was given two small finite displacements U_0 $=\pm0.02$ Å in the positive and negative directions. The elements of the force-constant matrix are the second derivatives of the ground-state total energy with respect to pair-wise combinations of the $3N$ coordinates. $D(\mathbf{q})$ has been obtained by taking the Fourier transform of the $3N\times3N$ force-constant matrix. In principle, the Fourier transform includes a term for every primitive cell in the macroscopic crystal, however, these contributions become very small beyond a cut-off distance. In the second step, for nonzero phonon wave vectors, we have calculated the force-constant matrix by assuming that the matrix elements of the real-space force-constant matrix become negligible for two atoms separated by a distance greater than the third nearest-neighbor distance of the framework lattice. Reference 23 gives a detailed discussion of this method. Once the force-constant matrix was obtained, $D(\mathbf{q})$ was obtained in the usual manner.

We have calculated the thermal properties of the clathrates of interest here in the usual manner. We have assumed that the system is a perfect crystalline lattice, that the only contribution to the entropy is the lattice vibrations and that the harmonic approximation is valid. Anharmonic effects are assumed to be small because all vibrational eigenvalues have been obtained at T=0 K.

In the harmonic approximation, the Helmholtz free energy F is given by

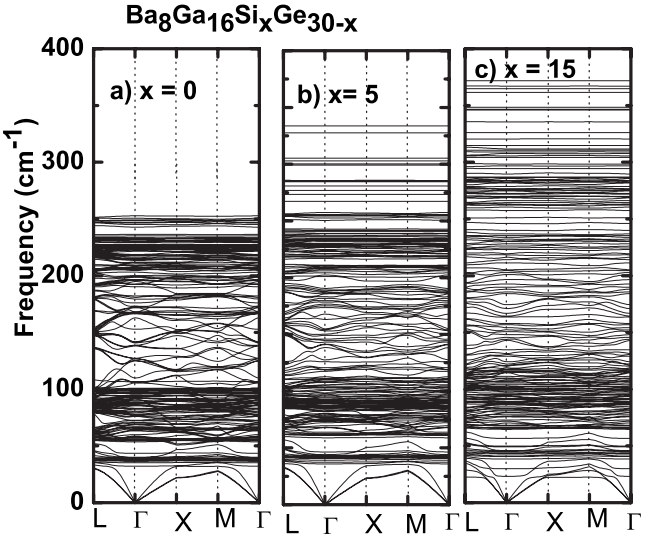

FIG. 1. Phonon-dispersion relations for the clathrates $Ba_8Ga_{16}Si_xGe_{30-x}$ for (a) $x=0$, (b) 5, and (c) 15.

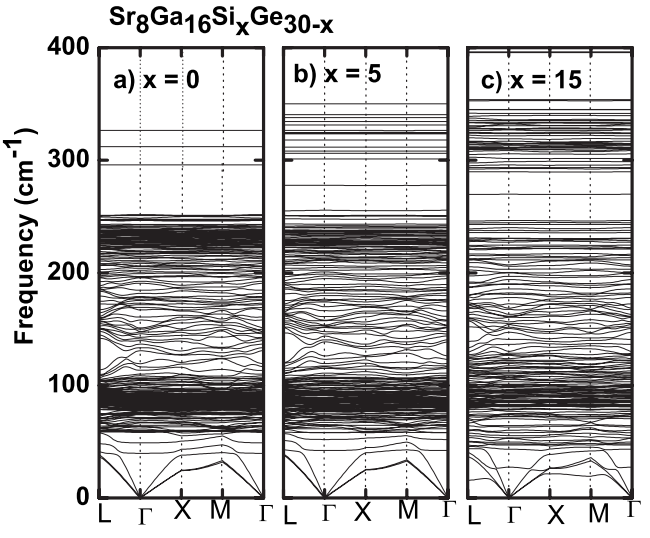

FIG. 2. Phonon-dispersion relations for the clathrates $Sr_8Ga_{16}Si_xGe_{30-x}$ for (a) $x=0$, (b) 5, and (c) 15.

$$F(V,T) = E(V) + F_{\text{vib}}(T) = E(V) + k_B T \sum_q \sum_j \ln\left\{2 \sinh\left(\frac{\hbar\omega_j(q)}{2k_B T}\right)\right\},$$

where E is the static contribution to the internal energy (obtained in the GGA), F_{vib} represents the vibrational contribution to the free energy, $\omega_j(q)$ is the frequency of the jth phonon mode at wave vector q in the Brillouin zone, k_B is Boltzmann's constant, and $\hbar$ is Planck's constant. In the same approximation, the vibrational entropy and the specific heat at constant volume are given by

$$S_{\text{vib}} = -\left(\frac{\partial F_{\text{vib}}}{\partial T}\right)_V \quad \text{and} \quad C_v = -T\left(\frac{\partial^2 F_{\text{vib}}}{\partial^2 T}\right)_V.$$

III. RESULTS AND DISCUSSION

A. Phonon dispersion relations and vibrational state densities

Lattice dynamics involve the collective motion of all atoms in the lattice. It is usually focused on the vibrational eigenvalues (squared vibrational frequencies) or phonon-dispersion curves. Our calculated dispersion curves for $Ba_8Ga_{16}Si_xGe_{30-x}$ are displayed in Figs. 1(a)–1(c) for $x=0$, 5, and 15, respectively. Those for $Sr_8Ga_{16}Si_xGe_{30-x}$ are shown in Figs. 2(a)–2(c) for $x=0$, 5, and 15, respectively. The dispersion curves are all similar to one another. In each material, there exist two high-densities of states regions. One region is just above the acoustic modes in the range $\sim 35-100$ cm^{-1} for the Ba-containing compounds and in the range $\sim 40-100$ cm^{-1} for the Sr-containing compounds. The other region is near the top of the optic branch above 200 cm^{-1} in both material types. Most of the optic bands are very flat, which is reminiscent of "zone folding." This effect becomes more pronounced as the silicon content increases. According to heat transport theory,[24] the flat optical modes will contribute very little to heat transport in the material.

One of the interesting features of these dispersion curves is the fact that the optic modes are slightly upshifted as the silicon concentration is increased. For $Ba_8Ga_{16}Si_xGe_{30-x}$, the highest optic modes are located at 253, 334, and 373 cm^{-1} for $x=0$, 5 and 15, respectively. For $Sr_8Ga_{16}Si_xGe_{30-x}$, they are located at 327, 350, and 428 cm^{-1} for $x=0$, 5 and 15, respectively. This upshift is larger in the upper optic bands, where the bond-stretching modes are located. This may be explained by noting that substitution of Ge atoms by Ga and Si strengthens the interatomic bonds. The GGA-calculated lattice constants for $A_8Ga_{16}Si_xGe_{30-x}$ from Ref. 13 show that the lattice constants in the Ba-containing compounds are slightly larger than those in the comparable Sr-containing materials. This is because the Ba atom is more massive than the Sr atom and it thus has a greater strain effect on the host. For both types of material, the lattice constant decreases as the number of silicon atoms on the framework increases. This is correlated with the fact that the silicon atom is smaller than both the gallium and germanium atoms. The calculated nearest-neighbor bond distances in $Ba_8Ga_{16}Si_xGe_{30-x}$ range from 2.53–2.63 Å and in $Sr_8Ga_{16}Si_xGe_{30-x}$ they range from 2.44–2.62 Å. In general, shorter bonds strengthen the structures, resulting in larger force constants.

A second interesting feature found in these results is the increase in the vibrational density of states (VDOS) at the bottom of the optic band just above the acoustic branches. The predicted VDOS curves are shown in Figs. 3(a) and 3(b) for $Ba_8Ga_{16}Si_xGe_{30-x}$ and $Sr_8Ga_{16}Si_xGe_{30-x}$, respectively, for $x=0$ and 5. A similar curve (not shown) is obtained for $x=15$. Our eigenvector analysis shows that these additional modes are coming from the guest atoms. In both figures, the VDOS is higher for $x=5$ than it is for $x=0$. The VDOS for $x=15$ (not shown in the figures) is the highest. The higher VDOS can be attributed to the smaller mass of the Sr atom in $Sr_8Ga_{16}Si_xGe_{30-x}$ in comparison to that of the Ba atom in $Ba_8Ga_{16}Si_xGe_{30-x}$. In comparison with the acoustic bandwidth in pristine Ge_{46} (Ref. 25) (which has an acoustic bandwidth of around 50 cm^{-1}), it is clear from the figures that

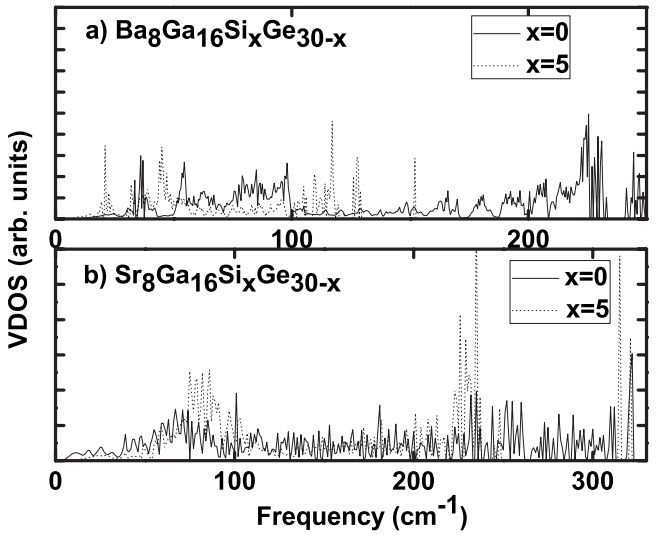

FIG. 3. The vibrational density of states for (a) $Ba_8Ga_{16}Si_xGe_{30-x}$ and (b) $Sr_8Ga_{16}Si_xGe_{30-x}$ for $x=0$ and 5.

these modes also compress the bandwidth of heat-carrying acoustic modes in $A_8Ga_{16}Si_xGe_{30-x}$. For $x=0$, 5 and 15, the tops of the acoustic bands in $Ba_8Ga_{16}Si_xGe_{30-x}$ are located at 33, 36, and 30 cm^{-1}, respectively. Similarly, in $Sr_8Ga_{16}Si_xGe_{30-x}$, the tops of the acoustic bands are located at 40, 42, and 33 cm^{-1} for $x=0$, 5 and 15, respectively. Thus, the acoustic bandwidths in $A_8Ga_{16}Si_xGe_{30-x}$ are reduced by about 16%–40%, depending on the value of x, in comparison to that of pristine Ge_{46}.

Because of an *avoided crossing effect*, there is a weak bonding of the guests residing inside the cages. This results in low-frequency-localized guest-atom vibrational modes which couple to the lattice modes by resonantly scattering the heat-carrying acoustic modes of the host framework.[6] Phonon modes near the region of the acoustic- to optic-mode transition range have a dual nature, which should allow thermal energy transfer from the framework to the guest atoms.[2] In Figs. 1 and 2, it is also important to note the gaps in the dispersion spectra within the optic bands. We also find these gaps in the vibrational densities of states. The presence of these gaps is an unusual feature in covalently bonded compounds. It was suggested by Kahn *et al.*[26] that in molecular solids, the high-energy intramolecular modes (due to the framework atoms) are separated from the low-energy intermolecular modes (guest-framework modes), which results in these gaps. This is a unique feature of clathrates and is likely caused by the open structure and interconnected cages of their lattices.

B. Effective potentials and effective force constants for guest motions

In order to help understand the type of motion that the guest atoms undergo in the small and large cages, we have calculated some guest-associated effective potential-energy curves. To calculate these, a single guest atom is displaced at a distance along a particular direction from its (*displaced from the cage center*) equilibrium position, while all other

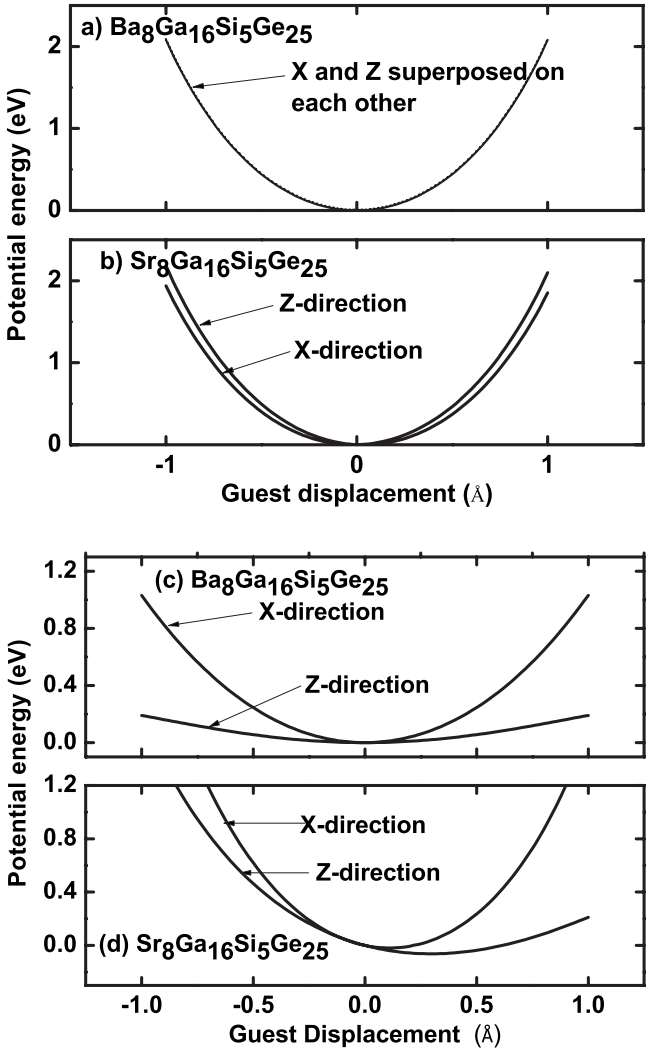

FIG. 4. The potential-energy curves for (a) Ba atom in the small 20-atom cage, (b) Sr atom in the small 20-atom cage, (c) Ba atom in the large 24-atom cage, and (d) Sr atom in the large 24-atom cage. X and Z represent the direction of motion of the guest atom.

atoms remain fixed and the total energy of the system for the guest in that new position is calculated. This is repeated for several displacements in the same direction, so that an energy versus displacement function (an effective potential-energy function) is generated for displacements along that direction. In the structure we have used, the Z axis is taken perpendicular to the hexagon of the 24-atom (large) cage and the X and Y axes are in a plane parallel to the plane of the hexagon. Due to the symmetry of the structure, the effective potential-energy curve for displacements along the X axis is identical to that along the Y axis. The details of this structure are discussed in Ref. 2.

The resulting effective potential-energy curves for guest-atom motions both in the X and Z directions for Si composition $x=5$ are shown in Figs. 4(a)–4(d). The potential-energy curve results for Ba guests moving in the small cages of $Ba_8Ga_{16}Si_5Ge_{25}$ are shown in Fig. 4(a) and those for Sr guests moving in the small cages of $Sr_8Ga_{16}Si_5Ge_{25}$ are shown in Fig. 4(b). Figures 4(c) and 4(d), respectively, show the effective potential-energy curve results for the motions of

TABLE I. Effective force constants (ϕ) from GGA-calculated frequencies (ω_{ph}) for the Ba guest atoms in $Ba_8Ga_{16}Si_xGe_{30-x}$ for $x=0$, 5, and 15, assuming the harmonic approximation and a rigid cage. The notation 1 for the guest location represents the guest atom in the small cage and the notation 2 represents the guest atom in the large cage. Also, θ_E is the Einstein temperature, which depends on the vibrational direction. $\theta_{E\text{-ave}}$ is the average Einstein temperature of guest atom in the clathrate obtained using the formula $(2\theta_{E1}+6\theta_{E2})/8$ where θ_{E1} is the average Einstein temperature in the small cages and θ_{E2} is the average Einstein temperature in the large cages.

x	Ba location and direction	ω_{ph} (cm^{-1})	ϕ (eV/Å^2)	θ_E (K)	$\theta_{E\text{-ave}}$ (K)
	1-X or Y	55.8	1.58	80	
	1-Z	57.0	1.61	82	
	2-X or Y	32.2	0.91	46	
0	2-Z	55.5	1.57	79	63
	1-X or Y	46.0	1.30	66	
	1-Z	72.1	2.04	103	
	2-X or Y	35.9	1.00	51	
5	2-Z	61.0	1.73	87	67
	1-X or Y	67.4	1.91	96	
	1-Z	75.9	2.15	109	
	2-X or Y	23.4	0.66	34	
15	2-Z	66.6	1.89	95	66

the Ba guests in the large cages of $Ba_8Ga_{16}Si_5Ge_{25}$ and of the Sr guests in the large cages of $Sr_8Ga_{16}Si_5Ge_{25}$. As can clearly be seen in Figs. 4(a)–4(d), the effective potential-energy functions for both Ba and Sr guest-atom motions are anisotropic and thus depend on whether the guest motion is along the X or the Z direction. Of the cases considered here, the effective potential-energy results which are most nearly isotropic are those [Fig. 4(a)] for the Ba guest motion in the small cages of $Ba_8Ga_{16}Si_5Ge_{25}$. For this case, the potential-energy curves for motion along the X and Z directions are nearly identical. From Fig. 4(b), the Sr guest motion in the small cages of $Sr_8Ga_{16}Si_5Ge_{25}$ is only slightly anisotropic; the potential-energy curves for X- and Z-directed motions only differ by about 0.1 eV at displacements of about 1.0 Å. By contrast, from Fig. 4(c), it is obvious that the potential-energy curves for the X and Z directed motions of Ba guests in the large cages of $Ba_8Ga_{16}Si_5Ge_{25}$ are very anisotropic; the potential-energy curves for the X and Z directed motions differ by more than 1.5 eV at displacements of about 1.0 Å. Similarly, Fig. 4(d) also clearly shows that the potential-energy curves for the X- and Z-directed motions of the Sr guests in the large cages of $Sr_8Ga_{16}Si_5Ge_{25}$ are also very anisotropic. Anisotropic behavior of the guests is also known to occur in types-I and II silicon clathrates.[27,28]

Related to the effective potential-energy function just discussed are the effective guest-host force constants ϕ. Using the GGA-calculated frequencies ω for the guest atoms, we have estimated the values of ϕ from the elementary relation $\omega=\sqrt{\phi/M}$, where M is the guest-atom mass. Of course, ϕ also depends on the direction of motion and on the type of

TABLE II. Effective force constants (ϕ) from GGA-calculated frequencies (ω_{ph}) for the Sr guest atom in $Sr_8Ga_{16}Si_xGe_{30-x}$ for $x=0$, 5, and 15. The remainder of the interpretation is the same as for Table I.

x	Sr location and direction	ω_{ph} (cm^{-1})	ϕ (eV/Å^2)	θ_E (K)	$\theta_{E\text{-ave}}$ (K)
	1-X or Y	35.8	0.42	52	
	1-Z	56.7	0.66	81	
	2-X or Y	29.2	0.34	42	
0	2-Z	66.3	0.78	95	60
	1-X or Y	43.6	0.51	62	
	1-Z	73.9	0.86	106	
	2-X or Y	42.2	0.49	60	
5	2-Z	63.5	0.74	91	72
	1-X or Y	74.9	0.87	107	
	1-Z	81.3	0.95	116	
	2-X or Y	27.3	0.32	39	
15	2-Z	43.3	0.51	62	63

cage just as the effective potential energy depends on these properties. As is shown in Tables I and II, we find that all values of ϕ for the Ba atoms in the small and large cages are larger than those for the Sr atoms in the same cages. Similar results for A_8Si_{46} (A=Na, K, I, or Ba) were obtained by Reny *et al.*[29] showing that Ba has the strongest-coupling constant with the host lattice. Furthermore, we find that ϕ for $Ba_8Ga_{16}Si_xGe_{30-x}$ is generally larger than ϕ for $Sr_8Ga_{16}Si_xGe_{30-x}$. This can be explained as follows. The Ba atom is larger than the Sr atom, so it is closer on the average to the framework atoms and it thus interacts more with the framework than the Sr atom. This is also consistent with the fact that the volume of the cage decreases as x increases. The guest atoms in the larger cages are obviously freer to move than those in the smaller cages. Further, though the Sr atom has smaller effective force constants than the Ba atom (see Tables I and II), it is 1.6 times less massive than Ba. We also note that these effective guest-atom force-constant values are very weak compared to those for the Ge-Ge bonds ($\sim$10 eV/Å^2).[2] It is worth noting that the vibrational frequency of the bond between the guest and the framework may be affected by the size of the cage.

C. Isotropic atomic displacement parameters and Einstein temperatures

For these same materials, we have calculated the isotropic atomic displacement parameters (ADP) for the guest atoms. The ADP is a measure of the mean-square displacement of an atom about its equilibrium position. The temperature-dependent isotropic mean-square displacement (U_{iso}) of the quantized harmonic oscillator is given by

$$U_{iso}=\langle u^2\rangle=\frac{h}{8\pi^2 m\upsilon}\coth\left(\frac{h\upsilon}{2k_BT}\right), \quad (1)$$

where υ is the vibrational frequency, m is the reduced mass of the oscillator, h is Planck's constant, T is the absolute

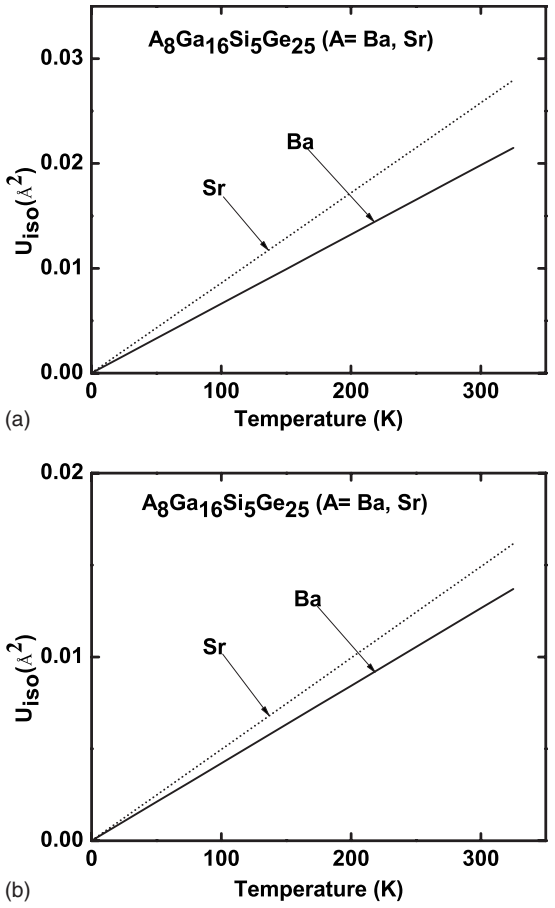

FIG. 5. Mean isotropic atomic displacement parameters (U_{iso}) as a function of temperature for guest atoms in $A_8Ga_{16}Si_xGe_{30-x}$ (A=Ba and Sr) for x=5 in (a) small and (b) large cages.

temperature, and k_B is Boltzmann's constant. Due to the rigidity of the framework, the guest-atom mass is assumed to be the reduced mass of the oscillator. At high temperatures ($h\upsilon \ll k_BT$), an estimate of the mean-square amplitude of the rattling guest atom can be estimated from the classical equation

$$U_{iso} \approx k_BT/\phi, \tag{2}$$

where ϕ is the effective force constant of the oscillator. The size of U_{iso} is correlated with amount of dynamic disorder of the atoms in the clathrate. We note that the expressions for U_{iso} in Eqs. (1) and (2) do not take into account static disorder effects resulting from the displacement of the guest-equilibrium positions from the cage centers. However, as discussed above, all of our GGA calculations do take this effect into account. Reference 30 reported that in alkaline-doped silicon clathrates, off-centered displacement depends on the coupling between the guest and the host. Including these effects in the calculation of U_{iso} would add a constant to the right sides of Eqs. (1) and (2) but would not affect the temperature dependence of the result. We thus ignore that constant in what follows. The larger the value of U_{iso}, the higher the probability of lowering the thermal conductivity.

Figure 5 shows the results obtained using Eq. (2) for the calculated mean ADP U_{iso} versus temperature in the range 0–325 K for the Ba and Sr guests in the clathrates in $A_8Ga_{16}Si_5Ge_{25}$ (A=Ba and Sr). Results for the Ba and Sr guests in the small (20 atom) cages and in the large (24 atom) cages are shown in Figs. 5(a) and 5(b). As can be seen in Fig. 5, the U_{iso} values for the Sr atoms are larger than those for the Ba atoms within the same temperature range. This result is in qualitative agreement with experiment[31] in materials, such as $Ba_8Ga_{16}Ge_{30}$, $Ba_8Ga_{16}Si_{30}$, $Ba_8In_{16}Ge_{30}$, and $Sr_8Ga_{16}Ge_{30}$. Because of the small size of the Sr atom compared to that of the Ba atom, the Sr atoms appear to be more off-centered than Ba atoms leading to a larger ADP.

Gatti *et al.*[32] carried out *ab initio* calculations on $Ba_8Ga_{16-z}Ge_{30+z}$ and $Sr_8Ga_{16-z}Ge_{30+z}$ with different Ga concentrations z. They have found that the guest-atom static disorder is due to an energy gain when many weak guest-host bonds in a symmetrical cage are replaced by a few much stronger and shorter bonds in an asymmetrical cage. These strong bonds are more directional in character than the weak bonds. This strong directional bonding is larger in $Sr_8Ga_{16}Ge_{30}$ than in $Ba_8Ga_{16}Ge_{30}$ which leads to higher guest-rattling frequencies in $Sr_8Ga_{16}Ge_{30}$ than in $Ba_8Ga_{16}Ge_{30}$.

On the basis of our results, we speculate that the Ba-rattling guests should be less efficient than the Sr guests in scattering the heat-carrying modes of the framework. This result is in agreement with that of Dong *et al.*[2] who showed that in $Cs_2Ba_6Ga_{14}Ge_{32}$ and $Rb_2Sr_6Ga_{14}Ge_{32}$, the Sr guest rattlers interact more strongly than the Ba guests with the heat-carrying acoustic modes of the framework just below the optic band, thus they have a higher probability of lowering the materials' thermal conductivity.

Because of their localized vibrational modes, the Ba and Sr guest atoms can approximately be treated as Einstein oscillators in these materials. However, there is a weak interaction between the guest modes and the framework atoms which is thought to lower the lattice thermal conductivity. Our predicted values for the Einstein temperature (θ_E) at T=0 K and the average Einstein temperature $\theta_{E\text{-ave}}$ for the Ba and Sr guest rattlers are shown in Tables I and II for $A_8Ga_{16}Si_xGe_{30-x}$ for x=0, 5, and 15. In those tables, $\theta_E = h\upsilon/k_B$ and $\theta_{E\text{-ave}}=(2\theta_{E1}+6\theta_{E2})/8$ where θ_{E1} and θ_{E2} are the average Einstein temperatures in the small and large cages. In the latter relation, the factors 2 and 6 denote the multiplicities of the small and the large cages, respectively. As is shown in Tables I and II, our predicted values for $\theta_{E\text{-ave}}$ in the Sr-containing materials are similar in size to those values in the Ba-containing materials.

It is worthwhile to compare our Einstein temperature results at x=0 with the experimental results reported in Ref. 31. There, it is reported that the average Einstein temperatures $\theta_{E\text{-ave}}$ are 64 K for Ba in $Ba_8Ga_{16}Ge_{30}$ and 80 K for Sr in $Sr_8Ga_{16}Ge_{30}$. Our prediction for $\theta_{E\text{-ave}}$ for the Ba guest in $Ba_8Ga_{16}Ge_{30}$ is 63 K, which is very close to the experimental value. Our calculated $\theta_{E\text{-ave}}$ for the Sr atom in $Sr_8Ga_{16}Ge_{30}$ is 60 K, or 25% smaller than that found in Ref. 31, but closer to the value of 53 K extracted from low-temperature heat-capacity data[33] and of 46 K obtained from the lowest Raman mode.[33] This discrepancy is consistent with our finding that the effective potential for Sr is anharmonic. It also indicates

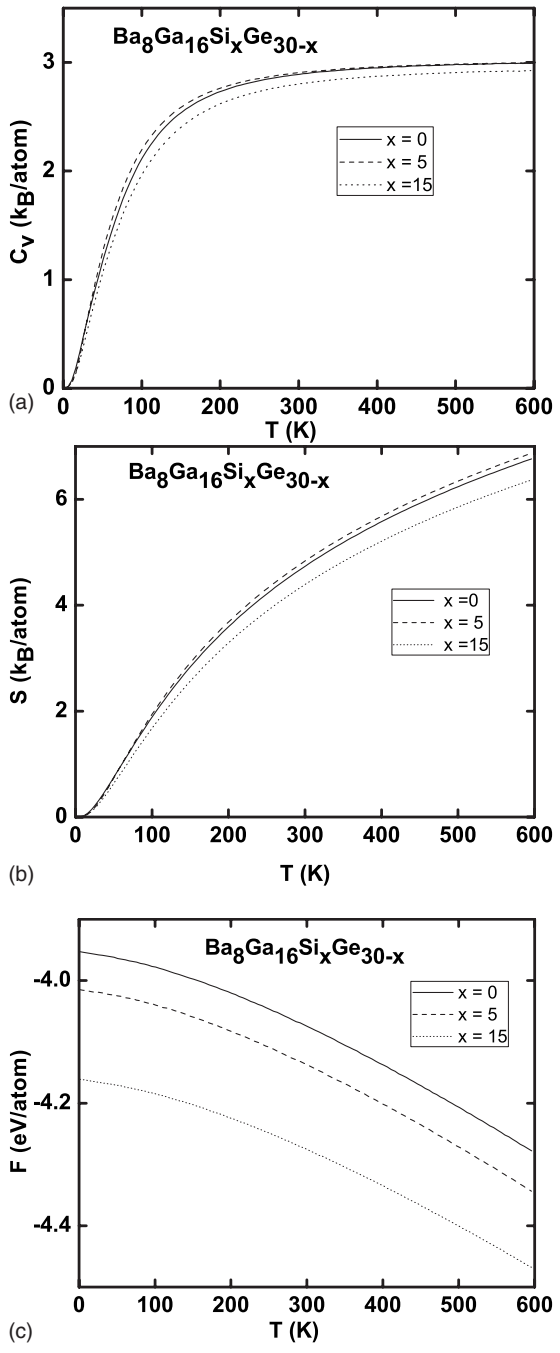

FIG. 6. Calculated thermal properties of $Ba_8Ga_{16}Si_xGe_{30-x}$ for $x=0$, 5, and 15 in the temperature range 0–600 K. (a) Specific heat at constant volume C_v, (b) vibrational entropy, and (c) vibrational free energy.

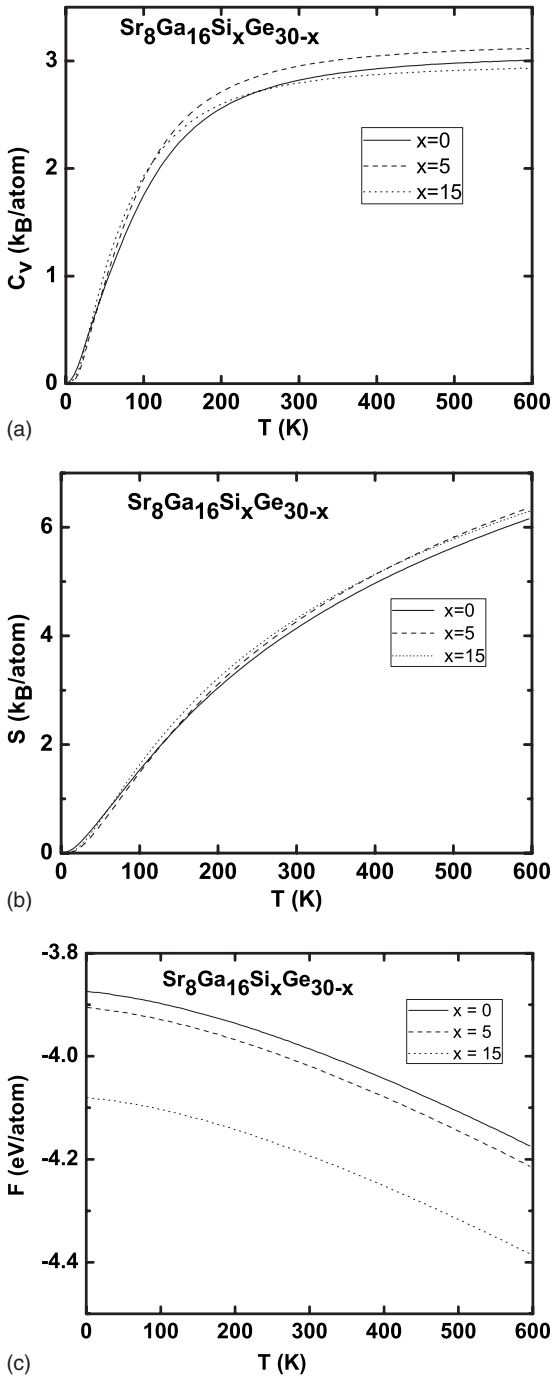

FIG. 7. Calculated thermal properties of $Sr_8Ga_{16}Si_xGe_{30-x}$ for $x=0$, 5, and 15 in the temperature range 0–600 K. (a) Specific heat at constant volume C_v, (b) vibrational entropy, and (c) vibrational free energy.

that it may not be correct to analyze the Sr ADP data using an isolated harmonic-oscillator model. However, this does not mean there is not a distinctive Einstein mode associated with the Sr motion. Instead, it means that in a simple analysis, θ_E cannot be easily determined using ADP data. In Ref. 31 static disorder (not included here) was found to be important in the analysis of the guest-atom ADP's in clathrates. In experiments on $Ba_8In_{16-x}Ge_{30-y\square x+y}$ (here, $\square$ represents a vacancy) and $Ba_8Ni_{6-x}Ge_{40-x}$ materials, it has been found[34] that the resonant scattering of host phonons by localized guest modes occurs at temperatures above ~50–70 K. From Tables I and II, it can be seen that our predicted values for $\theta_{E\text{-ave}}$ of the Sr and Ba guests are all above 59 K. This may imply that resonant scattering of host phonons would be dominant at temperatures above about 59 K.

D. Thermal properties

We have calculated the vibrational contributions to the specific-heat capacity, the entropy, and the Helmholtz free

energy of these same materials as a function of temperature. As we have shown in Secs. III A and III C, the guests in $A_8Ga_{16}Si_xGe_{30-x}$ vibrate at very low frequencies and therefore contribute little to either the heat capacity or to the other thermodynamic functions. Liyan *et al.*[35] showed that over a range of temperatures, there is little difference in specific heat at constant pressure (C_p) for $Sr_8Ga_{16}Ge_{30}$ and for $Ba_8Ga_{16}Si_{30}$. Our calculations are consistent with this. Figures 6(a) and 7(a) display, for $x=0$, 5, and 15, our predictions for the temperature dependence of the specific heat (C_v) for $Ba_8Ga_{16}Si_xGe_{30-x}$ [Fig. 6(a)] and $Sr_8Ga_{16}Si_xGe_{30-x}$ [Fig. 7(a)]. In lattice dynamics, the heat capacity at constant volume (C_v) is more easily calculated than C_p, which is usually measured in experiments. For solids, these quantities are related by $C_p - C_v = KTV\alpha^2$, where α is the volume coefficient of thermal expansion, K is the bulk modulus, T is the absolute temperature, and V is the volume. The difference between C_p and C_v in Na_8Si_{46} has been found in Ref. 36 to be about 5% at room temperature and to decrease in less than 0.1% at 100 K. This suggests that it is reasonable to compare C_p and C_v in most cases for temperatures up to around 300 K.

Figures 6(a)–6(c) show our predicted temperature dependences of the specific heat, the vibrational entropy, and the vibrational free energy, respectively, for $Ba_8Ga_{16}Si_xGe_{30-x}$ for $x=0$, 5, and 15. Figures 7(a)–7(c) show the comparable results for $Sr_8Ga_{16}Si_xGe_{30-x}$. The temperature dependences of each of these functions are qualitatively similar to each other. The C_v graphs [Figs. 6(a) and 7(a)] in both materials increase smoothly with temperature in the range 0–300 K. At about 300 K, C_v begins to approach the Dulong and Petit value of $3NR$, where R is the gas constant and N is the number of atoms in the unit cell. The C_v function flattens out as the temperature increases above about 300 K. This suggests that the optic and acoustic modes of these clathrates are fully excited at room temperature. As is seen in the figures, we predict that the dependence of C_v on x for a given temperature is very small. For example, we find that at $T=301$ K, C_v for $Ba_8Ga_{16}Si_xGe_{30-x}$ is 2.82, 2.96, and 2.80 k_B/atom for $x=0$, 5, and 15, respectively. For $Sr_8Ga_{16}Si_xGe_{30-x}$, at $T=301$ K, our predicted heat capacities are 2.82, 2.96, and 2.80 k_B/atom for $x=0$, 5, and 15, respectively.

Figures 6(b) and 7(b) show our predicted temperature dependences of the vibrational entropies for $Ba_8Ga_{16}Si_xGe_{30-x}$ and $Sr_8Ga_{16}Si_xGe_{30-x}$, respectively, for $x=0$, 5, and 15. At $T=301$ K, for $Ba_8Ga_{16}Si_xGe_{30-x}$, our calculated vibrational entropies are 4.75, 4.85, and 4.40 k_B/atom for $x=0$, 5, and 15, respectively. For $Sr_8Ga_{16}Si_xGe_{30-x}$, at the same temperature and x value, our predicted entropies are 4.15, 4.27, and 4.32 k_B/atom. As x increases, the vibrational entropy is expected to increase because of the increase in the vibrational frequencies with x. However, as we have found from the vibrational densities of states [Figs. 3(a) and 3(b)], the increase in the number of flat optics modes is very small and their intensities are very weak. This is thus unlikely to appreciably change the system's entropy. However, the reduction in unit cell size as x increases should lead to higher entropy. Since Sr-containing compounds have smaller sizes compared to their Ba counterparts, anharmonic effects on the guest modes can be quite different in these structures, especially at higher temperatures.

Figure 6(c) shows our results for the Helmholtz free energy as a function of temperature in $Ba_8Ga_{16}Si_xGe_{30-x}$ for $x=0$, 5, and 15, while Fig. 7(c) shows our prediction for this same function in $Sr_8Ga_{16}Si_xGe_{30-x}$ for these same x values. The free energy of a material strongly depends on the geometry of the atomic configurations. Figures 6(c) and 7(c) predict that as x increases, the material becomes thermodynamically more stable. From these figures, it can also be seen that the Ba-containing clathrates are predicted to be more stable than the Sr-containing compounds.

IV. CONCLUSIONS

We have calculated the vibrational and thermal properties of the clathrates $A_8Ga_{16}Si_xGe_{30-x}$ (A=Ba and Sr). Our calculated phonon-dispersion curves show that the rattling guest-atoms Ba and Sr tend to suppress the acoustic bandwidth of the host, therefore potentially lowering the material thermal conductivity. We also predict that Ba should be less effective than Sr in this suppression of the acoustic bandwidth. This is consistent with the relatively small isotropic displacement parameter we have found for Ba and should make it inefficient in scattering the heat-carrying phonons of the host. We also have found that the Einstein temperature has a small dependence on x. This effect is due to the increasing guest-atom vibrational frequencies as Ge atoms are replaced on the framework with Si atoms. A prediction on a trend in Einstein temperature with increasing x cannot be definitively established with the limited configurations we have considered. Finally, we have calculated the temperature dependences of the specific heat, the vibrational entropy, and the Helmholtz free energy of $A_8Ga_{16}Si_xGe_{30-x}$ (A=Ba and Sr) for $x=0$, 5, and 15. Our results show temperature variations of these functions which are similar to those found for other clathrate materials.[33–36] We note that experimenters have shown that thermoelectric properties depend a lot on sample preparation.[1,37]

ACKNOWLEDGMENTS

We thank M. Sanati (Texas Tech University) for useful discussions about the use of the VASP code for our calculations. We also thank G. S. Nolas (University of South Florida) for many helpful discussions on experimental trends in clathrate structures. We acknowledge many useful discussions about clathrate materials and the VASP code with Koushik Biswas (National Renewable Energy Laboratory). Finally, we thank Texas Tech University for many hours of computing time at the High Performance Computing System.

[1] J. Martin, S. Erickson, G. S. Nolas, P. Alboni, T. M. Tritt, and J. Yang, J. Appl. Phys. **99**, 044903 (2006), and references therein; J. Martin, G. S. Nolas, H. Wang, and J. Yang, *ibid.* **102**, 103719 (2007).

[2] J. Dong, O. F. Sankey, G. K. Ramachandran, and P. F. McMillan, J. Appl. Phys. **87**, 7726 (2000).

[3] K. Moriguchi, S. Munetoh, and A. Shintani, Phys. Rev. B **62**, 7138 (2000).

[4] N. P. Blake, L. Møllnitz, G. Kresse, and H. Metiu, J. Chem. Phys. **111**, 3133 (1999).

[5] N. P. Blake, S. Latturner, J. D. Bryan, G. D. Stucky, and H. Metiu, J. Chem. Phys. **115**, 8060 (2001).

[6] G. S. Nolas, G. A. Slack, and S. B. Schujman, in *Recent Trends in Thermoelectric Materials Research I*, Semiconductors and Semimetals Vol. 69, edited by T. M. Tritt (Academic, San Diego, 2000), and references therein.

[7] T. M. Tritt, in *Recent Trends in Thermoelectric Materials Research II*, Semiconductors and Semimetals Vol. 70, edited by R. K. Willardson and E. R. Weber (Academic, San Diego, 2001).

[8] G. A. Slack, in *CRC Handbook of Thermoelectrics*, edited by D. M. Rowe (CRC, Boca Raton, 1995), pp. 407–440.

[9] G. A. Slack, in *Proceedings of Thermoelectric Materials: New Directions and Approaches*, MRS Symposia Proceedings No. 478 (Materials Research Society, Pittsburgh, 1997), p. 47.

[10] G. S. Nolas, D. T. Morelli, and T. M. Tritt, Annu. Rev. Mater. Sci. **29**, 89 (1999).

[11] G. S. Nolas, J. L. Cohn, G. A. Slack, and S. B. Schujman, Appl. Phys. Lett. **73**, 178 (1998).

[12] J. Dong, O. F. Sankey, and C. W. Myles, Phys. Rev. Lett. **86**, 2361 (2001).

[13] E. N. Nenghabi and C. W. Myles, Phys. Rev. B **77**, 205203 (2008).

[14] J. D. Bryan, N. P. Blake, H. Metiu, G. D. Stucky, B. B. Iversen, R. D. Poulsen, and A. Bentien, J. Appl. Phys. **92**, 7281 (2002).

[15] D. Vanderbilt, Phys. Rev. B **41**, 7892 (1990).

[16] G. Kresse and J. Hafner, J. Phys.: Condens. Matter **6**, 8245 (1994); G. Kresse and J. Hafner, Phys. Rev. B **48**, 13115 (1993).

[17] Y. Wang and J. P. Perdew, Phys. Rev. B **44**, 13298 (1991).

[18] H. J. Monkhorst and J. D. Pack, Phys. Rev. B **13**, 5188 (1976).

[19] F. Birch, J. Geophys. Res. **57**, 227 (1952).

[20] The Birch Murnaghan equation for the energy E as a function of volume $E(V)=E_0+\frac{9}{8}KV_0[(\frac{V_0}{V})^{2/3}-1]^2\{1+[\frac{4-K'}{2}][1-(\frac{V_0}{V})^{2/3}]\}$, where E and E_0 are the energy and minimum energy, V and V_0 is the volume and volume at the minimum energy, K and K' are the bulk modulus and its pressure derivative.

[21] G. K. H. Madsen and G. Santi, Phys. Rev. B **72**, 220301(R) 2005.

[22] M. Christensen, N. Lock, J. Overgaard, and B. B. Iversen, J. Am. Chem. Soc. **128**, 15657 (2006).

[23] J. Dong, O. F. Sankey, and G. Kern, Phys. Rev. B **60**, 950 (1999).

[24] N. W. Ashcroft and N. D. Mermin, *Solid State Physics* (Holt, Reinhart, and Winston, New York, 1976), p. 500.

[25] J. Dong and O. F. Sankey, J. Phys.: Condens. Matter **11**, 6129 (1999).

[26] D. Kahn and J. P. Lu, Phys. Rev. B **56**, 13898 (1997).

[27] F. Brunet, P. Melinon, A. San Miguel, P. Keghelian, A. Perez, A. M. Flank, E. Reny, C. Cros, and M. Pouchard, Phys. Rev. B **61**, 16550 (2000).

[28] R. Lortz, R. Viennois, A. Petrovic, Y. Wang, P. Toulemonde, C. Meingast, M. M. Koza, H. Mutka, A. Bossak, and A. S. Miguel, Phys. Rev. B **77**, 224507 (2008).

[29] E. Reny, A. San-Miguel, Y. Guyot, B. Masenelli, P. Melinon, L. Saviot, S. Yamanaka, B. Champagnon, C. Cros, M. Pouchard, M. Borowski, and A. J. Dianoux, Phys. Rev. B **66**, 014532 (2002).

[30] H. Libotte, J. P. Gaspard, A. S. Miguel, and P. Melinon, Europhys. Lett. **64**, 757 (2003).

[31] A. Bentien, E. Nishibori, S. Paschen, and B. B. Iversen, Phys. Rev. B **71**, 144107 (2005).

[32] C. Gatti, L. Bertini, N. P. Blake, and B. B. Iverson, Chem.-Eur. J. **9**, 4556 (2003).

[33] G. S. Nolas and C. A. Kendziora, Phys. Rev. B **62**, 7157 (2000).

[34] A. Bentien, S. Johnsen, and Bo B. Iversen, Phys. Rev. B **73**, 094301 (2006).

[35] L. Qiu, I. P. Swainson, G. S. Nolas, and M. A. White, Phys. Rev. B **70**, 035208 (2004).

[36] L. Qiu, M. A. White, Z. Li, J. S. Tse, C. I. Ratcliffe, C. A. Tulk, J. Dong, and O. F. Sankey, Phys. Rev. B **64**, 024303 (2001).

[37] I. Fujita, K. Kishimoto, M. Sato, H. Anno, and T. Koyanagi, J. Appl. Phys. **99**, 093707 (2006).